Journal of Magnetic Resonance 206 (2010) 20–31

Contents lists available at ScienceDirect

Journal of Magnetic Resonance

journal homepage: www.elsevier.com/locate/jmr

Mellin transform of CPMG data

Lalitha Venkataramanan *, Fred K. Gruber, Tarek M. Habashy, Denise E. Freed

Schlumberger-Doll Research, One Hampshire Street, Cambridge, MA 02139, USA

ARTICLE INFO

Article history:
Received 9 March 2010
Revised 20 May 2010
Available online 9 June 2010

Keywords:
Inverse Laplace transform
Moment estimation
Analysis of CPMG data
Analysis of sum of exponentials
Fractional calculus
Mellin Transform

ABSTRACT

This paper describes a new method for computing moments of the transverse relaxation time T_2 from measured CPMG data. This new method is based on Mellin transform of the measured data and its time-derivatives. The Mellin transform can also be used to compute the cumulant generating function of $\ln T_2$. The moments of relaxation time T_2 and $\ln T_2$ are related to petro-physical and fluid properties of hydrocarbons in porous media. The performance of the new algorithm is demonstrated on simulated data and compared to results from the traditional inverse Laplace transform. Analytical expressions are also derived for uncertainties in these moments in terms of the signal-to-noise ratio of the data.

1. Introduction

In the past decade, NMR relaxation measurements using the CPMG pulse sequence have been used to probe the pore-geometry and fluid properties of hydrocarbons in porous media in grossly inhomogeneous fields [1]. The acquired data are represented by

$$M(t) = \int_0^\infty e^{-t/T_2} f_{T_2}(T_2) dT_2 + \epsilon(t), \quad t = [1, 2, \ldots, N] t_E. \tag{1}$$

The time constants T_2 are often assumed to be a continuum. Without loss of generality, the corresponding non-negative amplitude $f_{T_2}(T_2)$ is referred to as the distribution of T_2 relaxation times. Here $\epsilon(t)$ denotes the additive white, Gaussian noise (WGN) with known statistics.

In Eq. (1), the measured data $M(t)$ is related to the Laplace transform of the unknown distribution $f_{T_2}(T_2)$. In several applications, the parameters of interest are specific moments of T_2, which are used to provide insight into the underlying physical process. For example, the negative 0.4-th moment of T_2 has been empirically related to petro-physical parameters such as irreducible water-saturation in rocks. Similarly, the 0.2-th moment of T_2 has been found to be a good predictor of rock permeability [2]. The mean of the T_2 distribution denoted by $\langle \ln T_2 \rangle$ is empirically related to rock permeability or hydrocarbon viscosity. The width of the T_2 distribution $\sigma_{\ln T_2}$ is related to the pore size distribution in rocks [1]. In the study of hydrocarbons using NMR, the average chain length of a hydrocarbon is related to the 0.8-th moment of T_2 relaxation time [3].

Traditionally, the inverse Laplace transform (ILT) is used to estimate $f_{T_2}(T_2)$ from $M(t)$. The moments of T_2 are then computed from the estimated T_2 distribution. However, it is well-known that the ILT is an ill-conditioned problem [4,5]. Small changes in $M(t)$ due to noise can result in widely different $f_{T_2}(T_2)$. The classical approach to the problem involves choosing the "smoothest" solution $f_{T_2}(T_2)$ that fits the data. This smooth solution is often estimated by minimizing a cost function Q with respect to the underlying f [6,7],

$$Q = \|M - Kf\|^2 + \alpha \|f\|^2, \tag{2}$$

where M is the measured magnetization data, K is the matrix of the discretized kernel e^{-t/T_2} and f is the discretized version of the underlying density function $f_{T_2}(T_2)$ in Eq. (1). The first term in the cost function is the least-squares error between the data and the fit from the model in Eq. (1). The second term denotes Tikhonov regularization and incorporates smoothness in the expected solution of the density function.

The mathematical definition of smoothness as well as the value of α are subjective. The parameter α denotes the compromise between the fit to the data and an *a priori* expectation of the density function. When α is too small, the inversion problem is unstable with small changes in $M(t)$ resulting in widely different estimates for $f_{T_2}(T_2)$. When α is too large, the solution does not sufficiently take the measured data into account. In this case, the estimated density function, $f_{T_2}(T_2)$ is stable, but results in a poor fit to the data. In the literature, there is a wide variety of recipes to choose α, including the "L" curve method, generalized and ordinary cross validation, the "S" curve method, predictive mean square error, and self-consistency methods [8–11]. These

* Corresponding author.
E-mail address: lvenkataramanan@slb.com (L. Venkataramanan).

1090-7807/$ - see front matter © 2010 Elsevier Inc. All rights reserved.
doi:10.1016/j.jmr.2010.05.015

different methods provide different values of α and result in different solutions $f_{T_2}(T_2)$, all of which provide reasonable fits to the data.

In this paper, we build on the work in companion papers to compute the moments of T_2 directly from the measured data [12,13]. These moments are computed using Mellin transform (MT) of $M(t)$ and its time-derivatives. In applications where the parameter T_2 spans decades, quantities such as $\langle \ln T_2 \rangle$ and $\sigma_{\ln T_2}$ are of immediate interest. The MT can also be used to compute the cumulant generating function of $\ln T_2$. In addition, expressions are derived for uncertainty in the moments due to additive noise in the measured data. This new method obviates the need to compute moments from $f_{T_2}(T_2)$ estimated by the ill-conditioned ILT method. The performance of the MT as well as expressions for uncertainty are validated via simulations.

This paper is organized as follows. In the next section, we describe applications of the Mellin transform to CPMG data. In Section 3, we present the implementation details to compute moments and associated uncertainties. In Section 4, we compare the performances of the MT method with the traditional ILT method on a number of simulations at different signal-to-noise ratios (SNRs).

2. Moment estimation of T_2 relaxation using Mellin Transform

In this section, we provide expressions for moments of T_2 as a function of the measured CPMG data using the Mellin transform. We also describe some of the salient properties of Mellin transform which are useful while analyzing CPMG data where the relaxation time T_2 may span decades. The ω-th moment of T_2 is defined as

$$\langle T_2^{\omega} \rangle \equiv \frac{\int_0^{\infty} T_2^{\omega} f_{T_2}(T_2) dT_2}{\int_0^{\infty} f_{T_2}(T_2) dT_2}, \quad \omega \in \mathbb{R}, \tag{3}$$

where the area $\int_0^{\infty} f_{T_2}(T_2) dT_2$ is referred to as the porosity,

$$\phi = \int_0^{\infty} f_{T_2}(T_2) dT_2. \tag{4}$$

In general, when the density function $f_{T_2}(T_2)$ is known, the moments of T_2 can be computed in a straight-forward manner from Eq. (3). However, in our problem, $f_{T_2}(T_2)$ is unknown. Our recent work described in [12,13] demonstrates that when the measured data and density function are related by Eq. (1), then $\langle T_2^{\omega} \rangle$ can be computed from a linear transformation of $M(t)$,

$$\langle T_2^{\omega} \rangle = \frac{(-1)^n}{\Gamma(\mu)\phi} \int_0^{\infty} t^{\mu-1} \left[\frac{d^n M(t)}{dt^n} \right] dt, \tag{5a}$$

$$\omega = \mu - n, \quad \text{with} \quad \begin{cases} n = 0 & \text{if } \omega > 0, \\ n = [-\omega] + 1 & \text{otherwise.} \end{cases} \tag{5b}$$

Here $\Gamma()$ represents the Gamma function; it is a generalization of the factorial function when ω is a non-integer. The notation $[\omega]$ refers to the integral part of the number ω. The contribution of variable ω is in two parts: a real number μ and an integer n where the mathematical operator $t^{\mu-1}$ is applied on the n-th derivative of the data. The variation of n and μ with ω is given in Eq. (5b) and shown in Fig. 1. For example,the 0.2-th moment of T_2, related to permeability may be computed using Eq. (5) as

$$\left\langle T_2^{0.2} \right\rangle = \frac{1}{\Gamma(0.2)\phi} \int_0^{\infty} t^{-0.8} M(t) dt. \tag{6}$$

Similarly, the (-0.4)-th moment of T_2 related to irreducible water-saturation in rocks can be computed as

$$\left\langle T_2^{-0.4} \right\rangle = \frac{-1}{\Gamma(0.6)\phi} \int_0^{\infty} t^{-0.4} \left[\frac{dM}{dt} \right] dt. \tag{7}$$

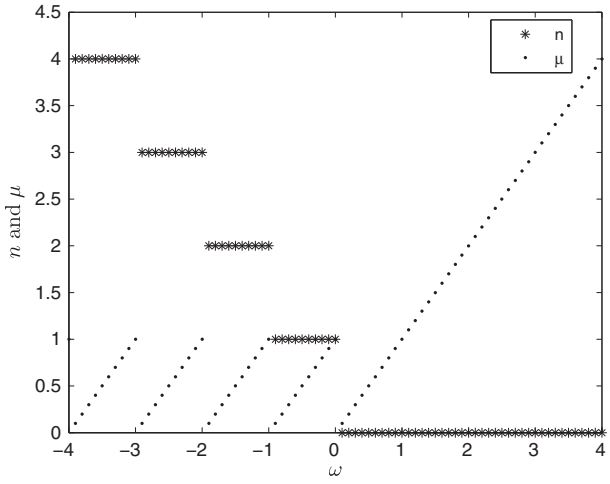

Fig. 1. Variation of n and μ with ω, as given by Eq. (5b). For example, when $\omega = -1$, $n = 2$ and $\mu = 1$. When $\omega = -0.2$, $n = 1$ and $\mu = 0.8$.

Eq. (5) can be proven from the perspective of fractional calculus. From Eq. (1), it is seen that integer moments of T_2 can be obtained by integration or differentiation of the data. For example,

$$\langle T_2 \rangle = \frac{1}{\phi} \int_0^{\infty} M(t) dt, \tag{8a}$$

$$\left\langle \frac{1}{T_2} \right\rangle = -\frac{1}{\phi} \left| \frac{dM}{dt} \right|_{t=0}, \tag{8b}$$

$$\left\langle \frac{1}{T_2^2} \right\rangle = \frac{1}{\phi} \left| \frac{d^2 M}{dt^2} \right|_{t=0}. \tag{8c}$$

A natural extension of Eq. (8) to fractional moments results in Eq. (5) where the regions $\omega > 0$ and $\omega \leqslant 0$ correspond to fractional integration and differentiation of the measured data, respectively [12].

Eq. (5) can also be proved from the definition of the Gamma function and the Mellin transform [13]. When the integral operator $t^{\mu-1}$ is applied to a signal $M(t)$, the resultant signal is referred to as the Mellin transform of $M(t)$ [14]. Thus, from Eq. (5), the positive moments of T_2 are obtained from the Mellin transform of $M(t)$. The negative moments are obtained from the Mellin transform of time-derivatives of $M(t)$.

As seen in Eq. (5), the fractional moments or Mellin transform results in a linear transformation of the measured data. In applications such as fluid characterization in porous media, where T_2 spans decades, the statistical properties of $\ln T_2$ are of direct interest. In this case, let

$$G(\omega) \equiv \ln \langle T_2^{\omega} \rangle. \tag{9}$$

The mathematical properties of $G(\omega)$ are described in [13]. First, $G(\omega = 0) = 0$. Second, as given in Eq. (1), when the data has asymptotically decayed to zero, $G(\omega)$ is a smooth, continuous function of ω. Lastly, $G(\omega)$ is the cumulant generating function of $\ln T_2$ with the first and second derivatives providing the mean and variance of $\ln T_2$,

$$\frac{dG}{d\omega}\Big|_{\omega=0} = \langle \ln T_2 \rangle, \quad \frac{d^2 G}{d\omega^2}\Big|_{\omega=0} = \sigma^2_{\ln T_2}. \tag{10}$$

Higher order cumulants of $\ln T_2$ are obtained by taking higher-order derivatives of $G(\omega)$ with respect to ω.

Fig. 2 illustrates these properties with examples. When $f_{T_2}(T_2)$ is the Dirac delta function with $\delta(T_2 - T_0)$, the corresponding $G(\omega)$ is a straight line with a slope of $\ln(T_0)$. When the density function is a

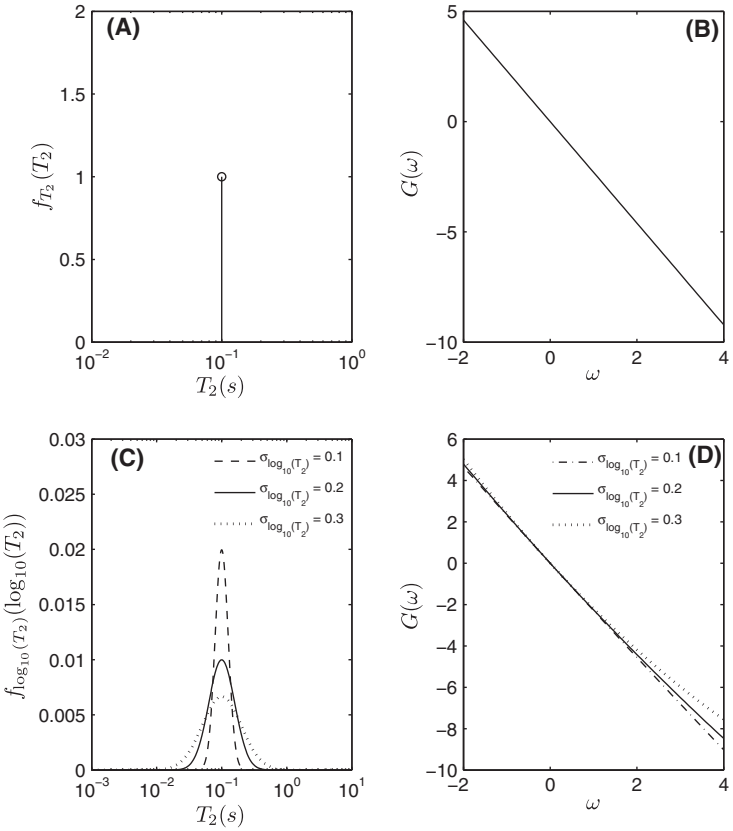

Fig. 2. Examples of two density functions and their cumulant generating functions. (A and B) The Dirac density function has a value of 1 at 0.1 s. The corresponding $G(\omega) = -2.3026\omega$. (C and D) $f_{\log(T)}$ is normal with $\langle \log_{10} T \rangle = 0.1$ s and $\sigma_{\log_{10}(T)} = 0.1$ (blue), 0.2 (green) and 0.3 (red). The corresponding $G(\omega)$ is a quadratic with $G(\omega) = \frac{\sigma^2_{\ln T_2}}{2}\omega^2 + \langle \ln T_2 \rangle \omega$. (For interpretation of the references to color in this figure legend, the reader is referred to the web version of this article.)

normal distribution with mean $\langle \ln T_2 \rangle$ and standard deviation $\sigma_{\ln T_2}$, the corresponding $G(\omega)$ is a quadratic function

$$G(\omega) = \frac{\sigma^2_{\ln\ T_2}}{2}\omega^2 + \langle \ln T_2 \rangle \omega. \tag{11}$$

Fig. 3 shows synthetic magnetization decay data $M(t)$ with additive noise together with the corresponding $G(\omega)$ computed using Eqs. (5) and (9). In addition to directly providing the ω-th moment of T_2, the slope and curvature of $G(\omega)$ at the origin yield $\langle \ln T_2 \rangle$ and $\sigma_{\ln T_2}$, respectively. Superimposed on $G(\omega)$ are the error-bars obtained from the MT analysis of data with different realizations of noise. Note that the error-bars are larger for negative values of ω. This is expected since the computation of negative moments involves taking time-derivatives of the data. Taking time-derivatives is akin to a high-pass filter operation and results in noisy estimates of the negative moments. A new method to get

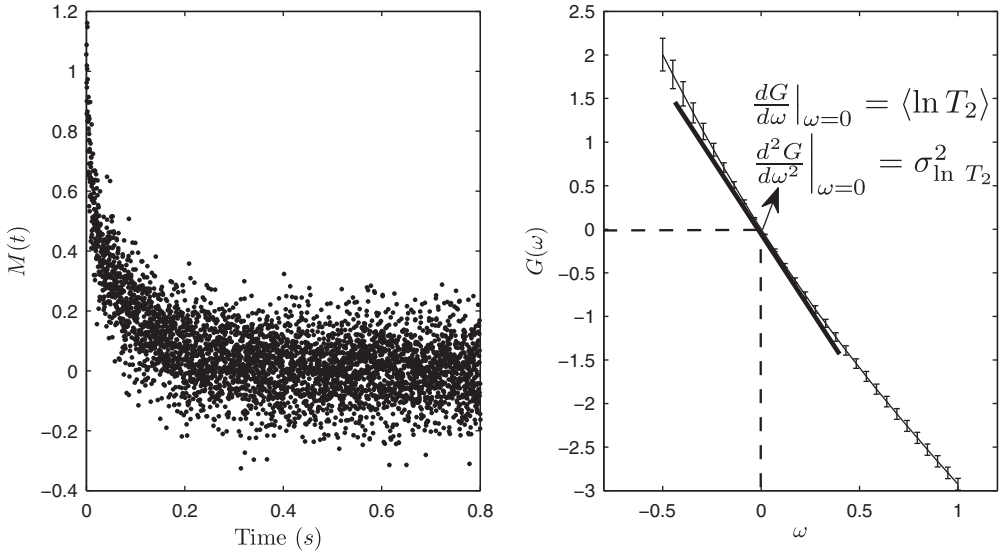

Fig. 3. (A) Simulated magnetization data at a poor signal-to-noise ratio. (B) Corresponding $G(\omega)$ computed using Eqs. (5) and (9). The function $G(\omega)$ is smooth and continuous and directly provides moments of T_2. It is also the cumulant generating function of $\ln T_2$.

around computing numerical derivatives is described in [13] and used in this figure to compute the negative moments. When the initial part of the data is well-characterized, this new method takes advantage of a Taylor-series expansion (TSE) of the initial decay along with re-writing of Eq. (5a). This helps provide a robust estimate and considerably decreases the error-bars in $G(\omega)$ for $\omega \leqslant 0$.

3. Implementation details

This section describes the implementation details for computing moments using Eq. (5). In addition, this section provides analytical expressions for the estimation of uncertainty in the moments due to uncertainty in the measured data due to additive noise. Let σ_ϵ denote the standard deviation of the noise at each echo. It is assumed that this parameter is known. Expressions for the uncertainty in moments of T_2 and $\ln T_2$ are derived in terms of the SNR ϕ/σ_ϵ of the data.

3.1. Estimate of porosity ϕ and associated uncertainty σ_ϕ

An important parameter required to compute the moments is the porosity ϕ. As seen from Eq. (4), porosity corresponds to the area under the T_2 distribution. From Eq. (1), it also corresponds to the unmeasured datum at $t = 0$. A commonly used method to compute porosity involved computing the complete T_2 distribution using the ILT method and computing its corresponding area. This method often results in an over-estimate of porosity. The approximate value of this bias can be pre-computed based on the SNR in the data and the porosity estimate corrected for the bias [15]. A second method involves Taylor-series expansion of the first few data points with extrapolation to $t = 0$. Let ϕ_1, σ_{ϕ_1} and ϕ_2, σ_{ϕ_2} denote the estimated porosities and associated uncertainties obtained from the two methods. In practice, both of these methods provide reasonable estimates of ϕ and σ_ϕ as long as there are no decays on the order of the echo-spacing t_E.

A straightforward weighted linear combination of the two estimates of porosity will have a variance smaller (or at worst the same) as that of the original estimates. Let a weighted-linear estimate of porosity be denoted by ϕ with standard deviation σ_ϕ,

$$\phi = \left(\frac{\sigma_{\phi_2}^2}{\sigma_{\phi_1}^2 + \sigma_{\phi_2}^2}\right)\phi_1 + \left(\frac{\sigma_{\phi_1}^2}{\sigma_{\phi_1}^2 + \sigma_{\phi_2}^2}\right)\phi_2, \tag{12}$$

$$\frac{1}{\sigma_\phi^2} = \frac{1}{\sigma_{\phi_1}^2} + \frac{1}{\sigma_{\phi_2}^2}. \tag{13}$$

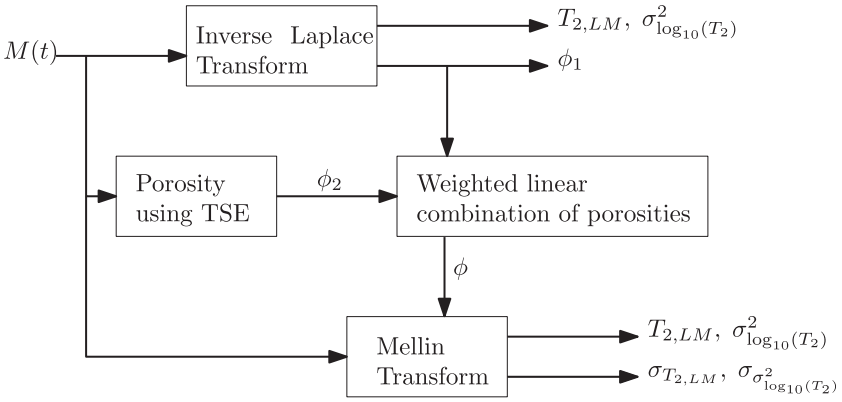

Fig. 4. The work flow used to compare MT and ILT methods. The data $M(t)$ is an input to both methods. The output of the ILT method is the T_2 distribution, from which its mean and width, $T_{2,LM}$ and $\sigma_{\log_{10}}(T_2)$ and porosity ϕ_1 are computed. In the MT, an additional input is the porosity ϕ which is computed as described in Section 3 as a weighted linear combination of the ILT method and Taylor-series expansion (TSE) of the initial decay. The output of the MT method are the mean and width of the T_2 distribution and associated uncertainties.

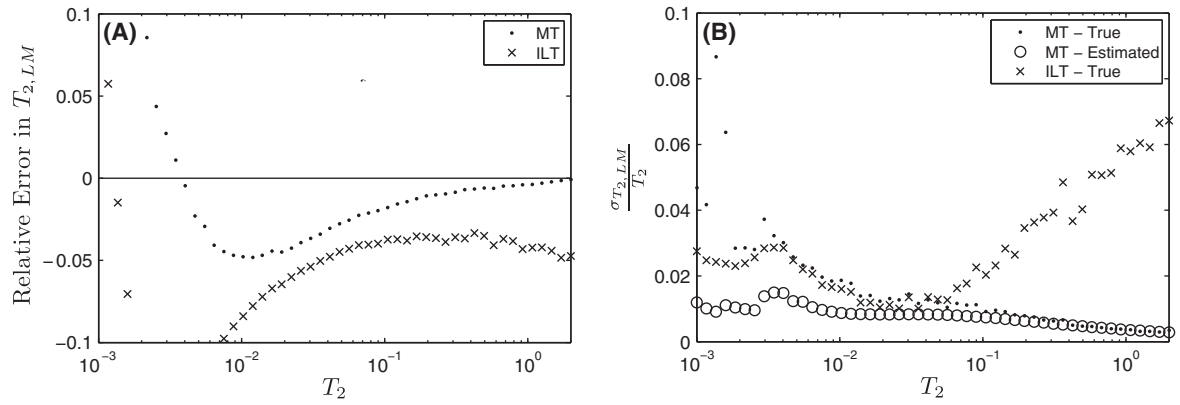

Fig. 5. Estimate of mean $T_{2,LM}$ of T_2 distribution from Dirac-delta model at high SNR: The MT has a lower bias and smaller variance in comparison to the ILT. In addition, the estimated standard deviation of parameter $T_{2,LM}$ matches the true standard deviation reasonably well.

The weights are chosen to provide an unbiased estimate and are based on the variances of the two porosity estimates: the smaller the variance of the estimated porosity, the larger the weight given to the estimate.

3.2. Estimate of uncertainty

Let a random variable y be a function of random variables $X = [x_1, x_2, \ldots, x_N]$. This sub-section provides expressions to

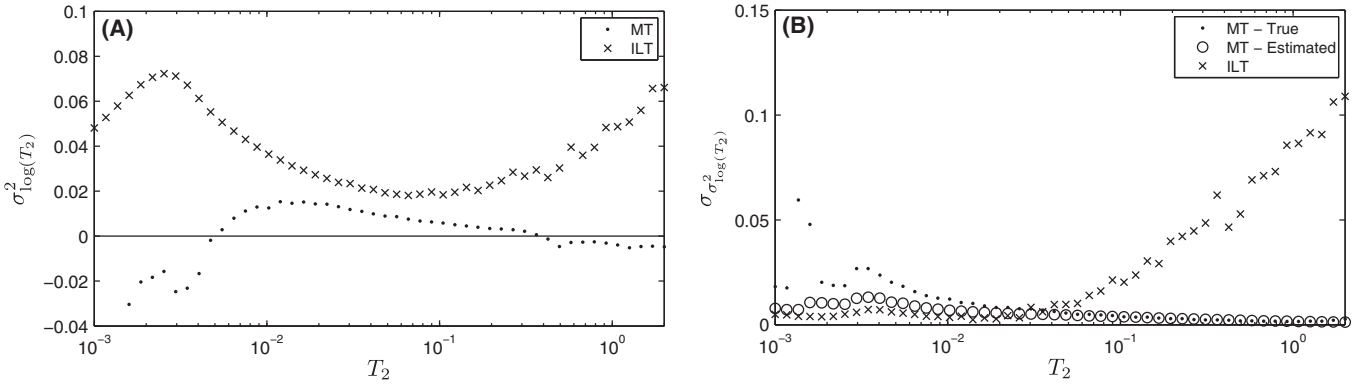

Fig. 6. Estimate of width $\sigma^2_{\log_{10}(T_2)}$ of T_2 distribution from Dirac-delta model at high SNR: The MT has (A) a lower relative error and (B) smaller variance in comparison to the ILT. The estimated standard deviation of the width matches the true standard deviation reasonably well.

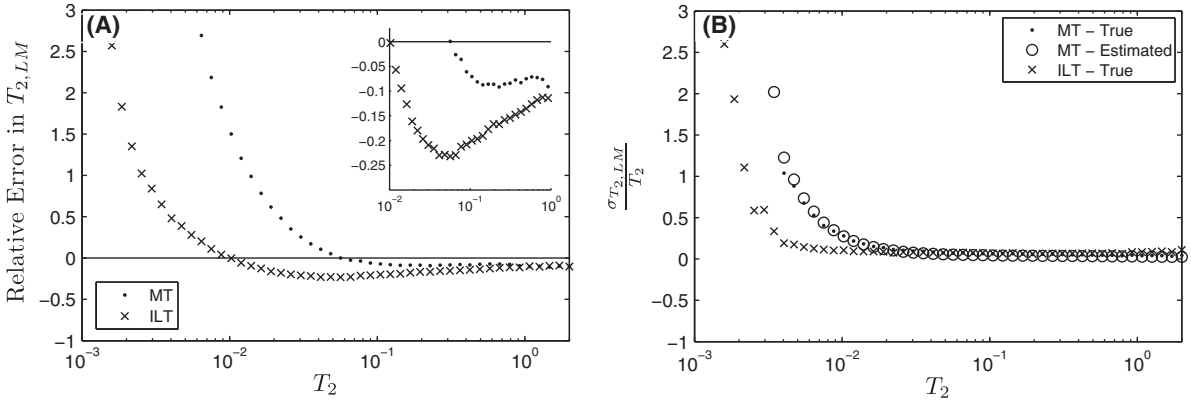

Fig. 7. Estimate of mean $T_{2,LM}$ of T_2 distribution from Dirac-delta model at low SNR: (A) At long relaxation times, the MT method has a slight edge over the ILT method. As shown in the zoomed-in plot, the average relative error from MT and ILT are about 10% and 17% respectively. At short relaxation times, the MT method does poorly due to poor estimate of porosity. (B) The estimated standard deviation of $T_{2,LM}$ matches the true standard deviation from ILT and MT reasonably well.

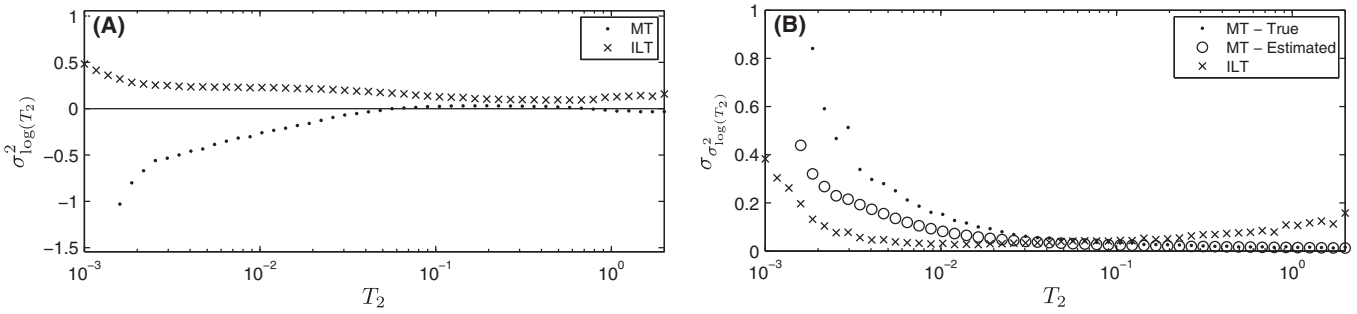

Fig. 8. Estimate of width $\sigma^2_{\log_{10}(T_2)}$ of T_2 distribution from Dirac-delta model at low SNR: The ILT has a comparable or lower bias and smaller variance in comparison to the MT. In addition, the estimated standard deviation of $\sigma^2_{\log_{10}(T_2)}$ matches the true standard deviation from ILT or MT reasonably well.

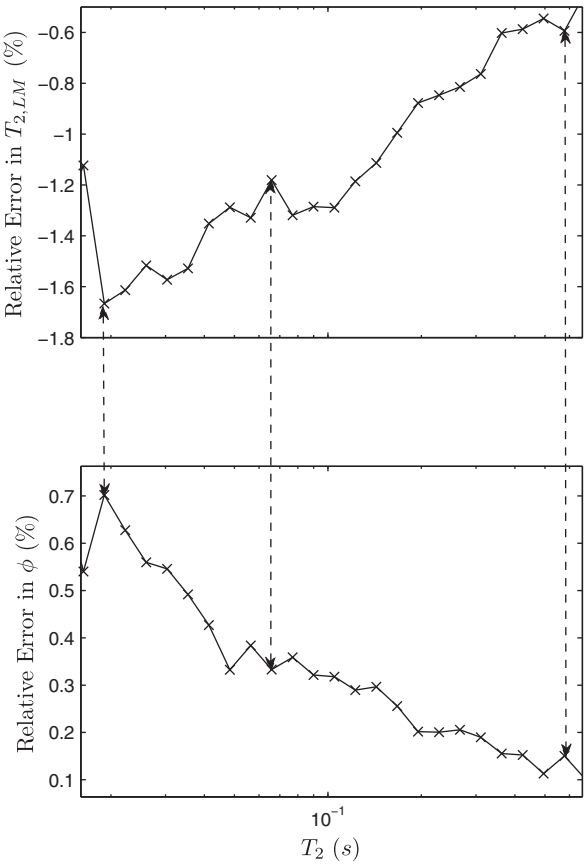

Fig. 9. From Eq. (5a), there exists an inverse correlation between porosity and estimated moments of T_2. Shown here is the relative error in $T_{2,LM}$ for Model A due to relative error in porosity.

compute the mean and variance of y in terms of the mean and covariance of X. Let

$$y = g(X). \tag{14}$$

Let η_X and Σ_X denote the mean and covariance of X, respectively. If the function $g()$ is approximated with a first-order Taylor-series expansion around its mean, then the mean and variance of y, denoted by η_y and σ_y^2, are

$$\eta_y \simeq g(\eta_X), \tag{15}$$

$$\sigma_y^2 \simeq J\Sigma_X J^T \quad \text{where} \quad J = \left[\frac{\partial g}{\partial x_1}\ \frac{\partial g}{\partial x_2}\cdots\frac{\partial g}{\partial x_N}\right]_{\eta_X}. \tag{16}$$

In the following sub-section, the variable y typically denotes the moments of $\langle T_2^\omega\rangle$. The variable X typically denotes the measured data, porosity, and information about initial time-decay (such as the slope at $t = 0$). Thus, using Eq. (16), the uncertainties in the moments are computed as a function of the uncertainties in the measured data, porosity, and slope at initial times. In turn, these uncertainties in the moments are translated into uncertainties in the parameters $\langle \ln T_2\rangle$ and $\sigma_{\ln T_2}$. Thus, we obtain analytic expressions for the uncertainties in moments in terms of the SNR ϕ/σ_ϵ and relative error in porosity ϕ/σ_ϕ.

3.3. Estimate of moments and their uncertainty

For a given value of ω, the moments are computed as follows.

Case 1: When $\omega = 0$, by definition, $\left\langle T_2^{\omega=0}\right\rangle = 1$.
Case 2: When $\omega > 0$, Eq. (5) yields

$$\langle T_2^\omega\rangle = \frac{1}{\Gamma(\omega)\phi}\int_0^\infty t^{\omega-1}M(t)dt. \tag{17}$$

By discretizing the integral in Eq. (17), this moment is computed as a weighted linear combination of the data [13],

$$\langle T_2^\omega\rangle = k + \frac{1}{\Gamma(\omega+1)\phi}\sum_{i=1}^{N}\Delta_i M(it_E), \tag{18}$$

where

$$k = \frac{\tau_{min}}{\Gamma(\omega+1)} \quad \text{is a constant,} \tag{19a}$$

$$\tau_{min} = t_E^\omega, \tag{19b}$$

$$\Delta_1 = 0.5t_E^\omega[2^\omega - 1^\omega], \tag{19c}$$

$$\Delta_i = 0.5t_E^\omega[(i+1)^\omega - (i-1)^\omega], \quad i = 2,\ldots,N-1 \tag{19d}$$

$$\Delta_N = 0.5t_E^\omega[N^\omega - (N-1)^\omega] \tag{19e}$$

Thus, for a given t_E and N, the positive moments are a straightforward linear transformation of the data.

Case 3: When $-1 < \omega < 0$, Eq. (5) yields

$$\langle T_2^\omega\rangle = \frac{-1}{\Gamma(\omega+1)\phi}\int_0^\infty t^\omega\left[\frac{dM}{dt}\right]dt \tag{20}$$

As mentioned previously, when the initial part of the data is well-characterized, a Taylor-series expansion of the initial decay can help provide a robust estimate of negative moments and considerably decrease the error-bars in $G(\omega)$ for $\omega \leqslant 0$ [13]. In this case, after a suitable integration by parts, Eq. (20) can be re-written as

$$\langle T_2^\omega\rangle = \frac{1}{\Gamma(\omega)\phi}\int_0^\infty t^{\omega-1}[M(t)-\phi]dt \tag{21}$$

This can also be implemented as a weighted linear combination of the data,

$$\langle T_2^\omega\rangle = k + \frac{1}{\Gamma(\omega+1)\phi}\left[\left(\frac{a_1\omega}{\omega+1}\right)\tau_{min}^{\frac{\omega+1}{\omega}} + \sum_{i=1}^{N}\Delta_i M(it_E)\right] \tag{22}$$

where k, τ_{min}, and Δ_i (for a given value of ω) are given in Eq. (19) and $a_1 = \frac{dM}{dt}\big|_{t=0}$. Thus, for a given t_E and N, the negative moments are also computed via a straightforward linear transformation of the data.

Since each moment is evaluated as the weighted linear combination of the data, the variance of each moment due to noise is also easily computed analytically. When $\omega > 0$, from Eqs. (16) and (18), we get

$$\sigma^2_{\langle T_2^\omega\rangle} = \frac{\sum_i \Delta_i^2}{\Gamma^2(\omega+1)}\left(\frac{\sigma_\epsilon}{\phi}\right)^2 + \left(\langle T_2^\omega\rangle - k\right)^2\left(\frac{\sigma_\phi}{\phi}\right)^2. \tag{23}$$

When $-1 < \omega \leqslant 0$, from Eqs. (16) and (22), we have

$$\sigma^2_{\langle T_2^\omega\rangle} = \frac{\sum_i \Delta_i^2}{\Gamma^2(\omega+1)}\left(\frac{\sigma_\epsilon}{\phi}\right)^2 + \left(\langle T_2^\omega\rangle - k\right)^2\left(\frac{\sigma_\phi}{\phi}\right)^2 + \left(\frac{\omega\tau_{min}^{\frac{\omega+1}{\omega}}}{\Gamma(\omega+2)}\right)^2\left(\frac{\sigma_{a_1}}{\phi}\right)^2. \tag{24}$$

The three terms in Eq. (24) are due to the uncertainties in the measured data, the estimated porosity, and the initial time-decay, respectively.

From the computed moments, the function $G(\omega) = \ln\langle T_2^\omega\rangle$ is easily computed. Let Σ_ω denote the diagonal covariance matrix of the moments computed using Eq. (23) for different values of ω. The covariance of $G(\omega)$ is computed using Eq. (16),

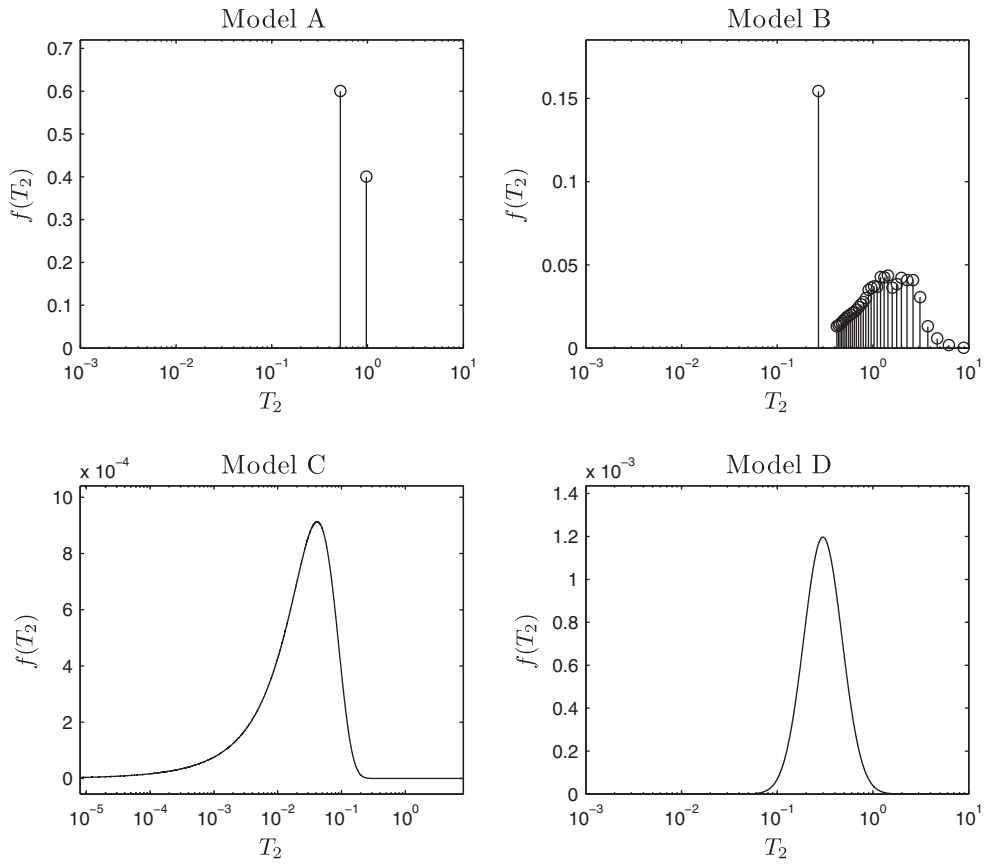

Fig. 10. Variety of simulation models were considered. Model B corresponds to the relaxation times of a synthetic mixture of C_{15} and C_{25} at 30 °C [3]. Models A–D were chosen to have different shapes and span different regions of the T_2 space.

$$\Sigma_G = J\Sigma_\omega J^T, \quad J = \left[\frac{1}{\langle T_2^{\omega_1}\rangle}\ \frac{1}{\langle T_2^{\omega_2}\rangle}\cdots\right]. \tag{25}$$

A weighted least squares quadratic fit to function $G(\omega)$ estimated for various discrete values of ω is used to directly provide $\langle \ln T_2\rangle$, $\sigma_{\ln T_2}$, and their corresponding standard deviations.

4. Simulation results

In this section, we have two main objectives. First, we evaluate and compare the performances of the MT method with the traditional ILT method. For simplicity, we compare their performances in estimating the mean and width of T_2 distributions. Second, we compare the estimated uncertainties in these parameters computed from expressions given in Section 3 with the true uncertainties. True uncertainties are obtained from the analysis of data consisting of the same underlying noiseless signal but combined with different noise realizations.

Noiseless data are simulated from specified T_2 distributions and corrupted with different levels of additive zero-mean, white, Gaussian noise with standard deviation σ_ϵ. The true porosity is unity. Random white Gaussian noise with $\sigma_\epsilon = 0.02$ or 0.2 was added to the noiseless signal to simulate noisy data representing data at high and low SNR, respectively.

The work flow used to compare MT and ILT methods is shown in Fig. 4. The noisy magnetization data $M(t)$ is an input to both methods. The outputs of the ILT method are the porosity and the mean and width of T_2, computed from the estimated T_2 distribution. To solve Eq. (2), the T_2 values were discretized at 100 logarithmically spaced points between $2t_E$ and 10 s. *20* singular values were chosen when the kernel e^{-t/T_2} was discretized. The data were analyzed with $\alpha = 1$ and 100 in Eq. (2) at the two SNRs, respectively. These values of α are typical for analyzing data at these SNRs.

In the MT method, an additional input is the porosity ϕ. This was computed as a weighted linear combination of ILT and Taylor-series expansion methods described briefly in Section 3. The output of the MT method are the mean and width of the T_2 distribution and associated uncertainties. In the MT method, the mean and width of the T_2 distribution are estimated from Eq. (10) where

Table 1
Parameters used to simulate data for models A–D.

Model number	t_E (μs)	N
A	800	8000
B	2000	6000
C	200	2000
D	500	5000

Table 2
Estimate of porosity at the two different SNRs. The means and standard deviations are obtained from 1024 different realizations of data simulated from each model.

Model	$\sigma_\varepsilon = 0.02$	$\sigma_\varepsilon = 0.2$
A	1 ± 0.002	1.01 ± 0.024
B	1 ± 0.004	1 ± 0.037
C	0.95 ± 0.011	0.89 ± 0.048
D	1 ± 0.003	1.01 ± 0.029

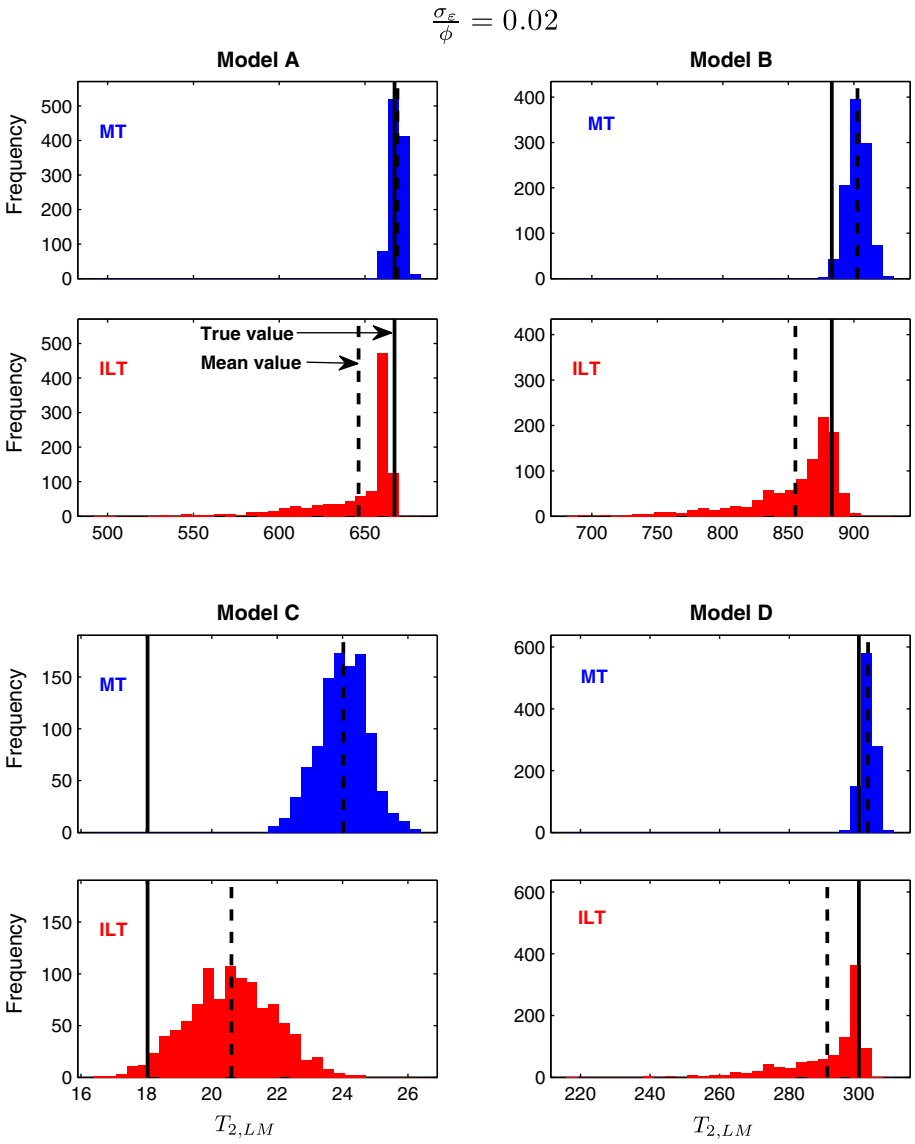

Fig. 11. Histograms of parameter $T_{2,LM}$ from analysis of 1024 data sets simulated from models A–D at high SNR: The true and mean values of $T_{2,LM}$ are indicated. With the exception of model C, the MT estimate of $T_{2,LM}$ has a lower bias and variance.

the first and second-order derivatives were computed with a weighted least squares quadratic fit of $G(\omega)$ using 30 discrete values of ω between -0.5 and 1.

Performances of the algorithms are based on two criteria: the bias and the variance of the estimated parameters. Bias denotes the relative error in a parameter estimate. The bias and variance are computed in reference to the true values from the mean and variance of the parameters obtained from analyzing data with multiple realizations of noise. An unbiased method with low variance is desirable.

4.1. Dirac-delta function

Data was simulated from Dirac-delta function in the T_2 domain, where the time constant of the delta function was varied systematically from 1 ms to 2 s. Synthetic single exponential echo-decay trains were simulated with $t_E = 500$ μs. Random white Gaussian noise with σ_ϵ was added to the noiseless signal to simulate noisy data. The data were analyzed with MT and ILT methods. The results are summarized in Figs. 5–9. We make the following observations:

1. Estimate of mean of T_2 distribution at high SNR: In applications where parameter T_2 spans decades, the parameter $T_{2,LM}$, defined as,

$$T_{2,LM} = 10^{\langle \log_{10}(T_2) \rangle}, \tag{26}$$

is used to denote the mean of the T_2 distribution [1]. Using the MT described in this paper, the parameter $\langle \log_{10}(T_2) \rangle$ was computed from the slope of the function $\log_{10}\langle T_2^\omega \rangle$. From Eq. (16), the uncertainty in $T_{2,LM}$ is obtained in terms of the mean and standard deviation of $\log_{10}(T_2)$,

$$\sigma_{T_{2,LM}} = (\ln 10) T_{2,LM} \sigma_{\langle \log_{10}(T_2) \rangle}. \tag{27}$$

The relative error in $T_{2,LM}$ as well as the estimated and true standard deviations (obtained from 400 noise realizations) are shown in Fig. 5. It is seen that the MT does reasonably well with an average of 2% relative error in comparison to the ILT method which has 8% relative error. The true and estimated standard deviations are shown in Fig. 5B. It is seen that the ILT method has a larger variance in comparison to the MT method. In addition, the estimated standard deviations com-

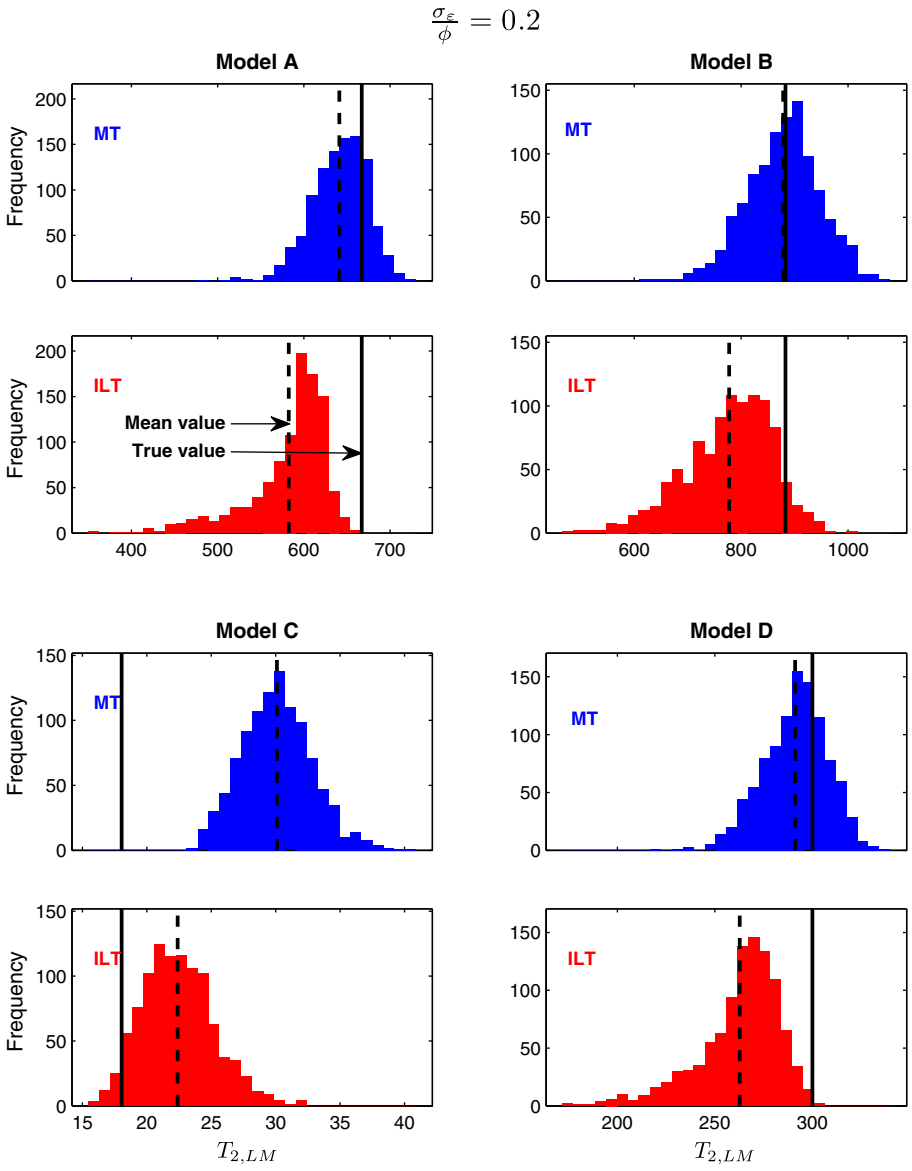

Fig. 12. Histograms of parameter $T_{2,LM}$ from analysis of 1024 data sets simulated from models A–D at low SNR: The true and mean values of $T_{2,LM}$ are indicated. With the exception of model C, the MT estimate of $T_{2,LM}$ has a lower bias and variance.

pare reasonably well with the true estimates of the standard deviation of the parameter for large values of T_2 when the porosity is estimated reasonably well.

2. Estimate of width of T_2 distribution $\sigma_{\log_{10}T_2}$ at high SNR: Since the T_2 distribution is a Dirac delta function, it has no width and the true value of $\sigma_{\log_{10}(T_2)}$ is zero. The bias in this parameter from MT and ILT is shown in Fig. 6A. The MT estimates the parameter to be close to zero, whereas there is a significant bias from the ILT method. Similarly, the estimated standard deviation of the parameter matches the true value reasonably well in Fig. 6B, whereas the ILT method estimates the parameter with a large variance.
3. Estimate of mean $T_{2,LM}$ at low SNR: At longer relaxation times when porosity is estimated well, the MT performs better than the ILT (see Fig. 7A). As shown in the zoomed plot, at these long relaxation times, the MT does reasonably well with an average of 10% relative error in comparison to the ILT method which has 15% relative error. However, at shorter relaxation times when the porosity is estimated poorly (for example, for $T_2 < 30$ ms), the ILT method outperforms the MT method. It is also observed in Fig. 7B that the estimated standard deviation of $T_{2,LM}$ matches that of MT at long relaxation times.
4. Estimate of width $\sigma_{\log_{10}(T_2)}$ at low SNR: The bias and variance in this parameter from MT and ILT is shown in Fig. 8A and B respectively. The MT method performs better with smaller bias and lower variance at long relaxation times. On the other hand, the ILT method has a slightly larger bias and a comparable variance for almost the entire spectrum of relaxation times. In Fig. 8B, at long relaxation times, the estimated standard deviation from the MT method matches the true standard deviation reasonably well.

These results highlight an important characteristic of the MT estimates: its sensitivity to the input porosity in Eq. (5). Fig. 9 further illustrates this showing the inverse correlation between the porosity and the $T_{2,LM}$ estimates for this model.

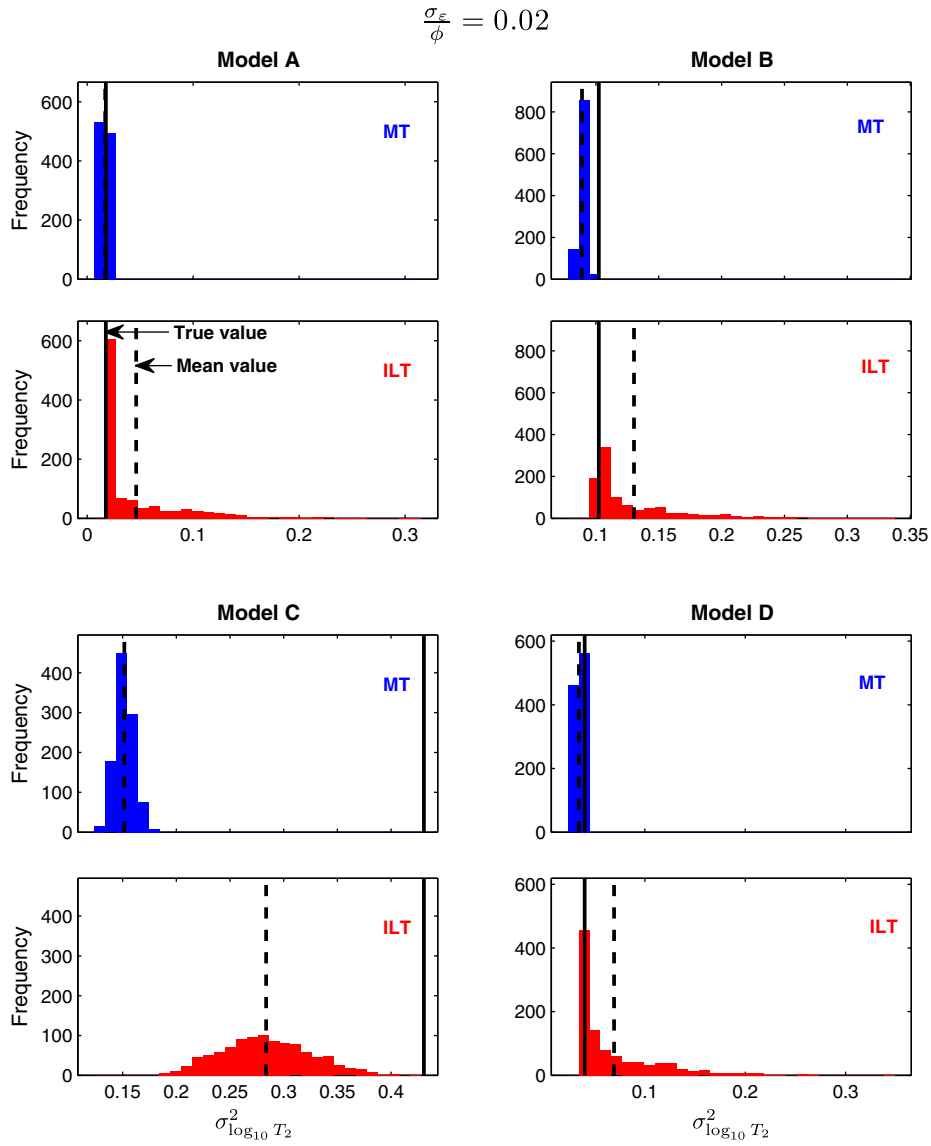

Fig. 13. Histograms of width $\sigma_{\log_{10}(T_2)}$ of T_2 distribution from analysis of 1024 data sets simulated from models A–D at high SNR: With the exception of model C, the MT outperforms the ILT method and has a lower bias and variance.

4.2. Models A–D

Consider various T_2 distributions as shown in Fig. 10. For ease of comparison, all distributions are normalized to have a porosity of unity. Noiseless signals were simulated from these distributions with parameters given in Table 1. White, Gaussian noise was added to these signals to simulate good and poorer quality data sets with $\sigma_\epsilon = 0.02$ and 0.2, respectively. The mean and variances for the different parameters were obtained from analysis of 1024 realizations of noise at each SNR for each model.

Estimated porosity for the different models and at the two SNRs is given in Table 2. We note that the estimate of porosity is unbiased with the exception of model C, where 2% of the porosity is below t_E and is, therefore, not measured.

The ILT and MT methods are used to analyze the data and estimate the mean $T_{2,LM}$ and width $\sigma^2_{\log_{10}(T_2)}$ of the T_2 distribution. The results of this analysis are summarized in two different ways. First, histograms of the parameters $T_{2,LM}$ and $\sigma^2_{\log_{10}(T_2)}$ obtained from analysis of 1024 data sets at two different SNRs are shown in Figs. 11–14. Second, these results are also summarized in Table 3.

We make the following observations:

1. Bias in $T_{2,LM}$: With the exception of model C (where the porosity is estimated with a bias), the MT method outperforms the ILT method. The bias (relative error) from the MT is much smaller than that from the ILT method. This is seen in Figs. 11 and 12 and Table 3. For example, the true value of $T_{2,LM}$ for model A is 667 ms. At high SNRs, the mean value of this parameter from MT and ILT methods are 669 and 646 ms, respectively.
2. Relative uncertainty in $T_{2,LM}$: The estimated uncertainty in $T_{2,LM}$ is computed from $\frac{\sigma_{T_{2,LM}}}{T_{2,LM}}$ using Eqs. (26) and (27). The true uncertainty is estimated from analysis of 1024 realizations of the data using MT and ILT methods. The true and estimated uncertainties compare reasonably well in Table 3. For example, for model A at high SNRs, the error-bar in $T_{2,LM}$ using the MT method be 1%. The estimated error-bar from Eq. (27) is 0.4% and is therefore a good approximation. On the other hand, the error-bar from the ILT method is about 4% and much larger than that from MT method.

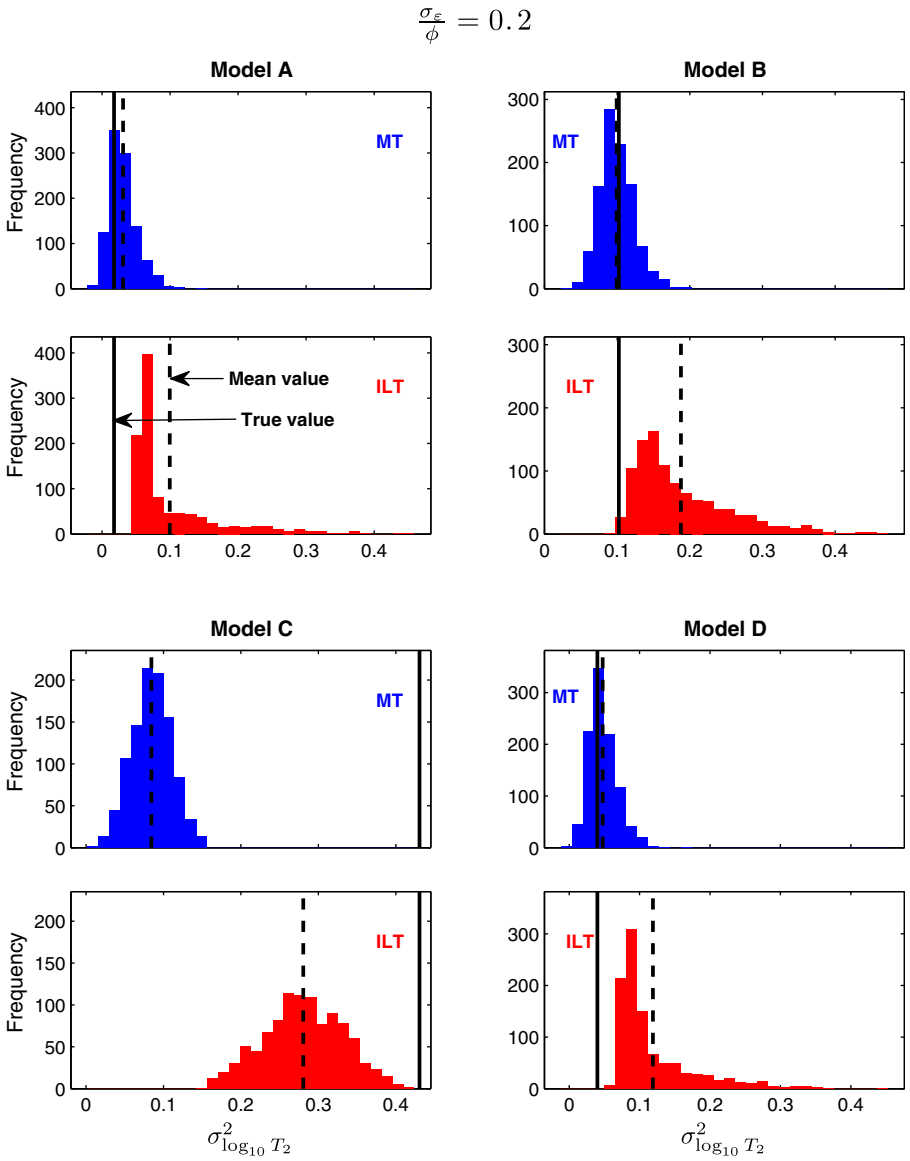

Fig. 14. Histograms of width $\sigma_{\log_{10}(T_2)}$ of T_2 distribution from analysis of 1024 data sets simulated from models A–D at low SNR: With the exception of model C, the MT outperforms the ILT method and has a lower bias and smaller variance.

3. Bias in $\sigma^2_{\log_{10} T_2}$: As seen in Figs. 13 and 14, the ILT method overestimates the width of the T_2 distribution (with the exception of model C). On the other hand, the MT method does a more reasonable and unbiased estimate of the width. For example, for model A at high SNRs, the true width is 0.02. The estimated width of 0.02 from MT matches the true width. The width from the ILT method is 0.05 and much larger than the true width.
4. Relative uncertainty in $\sigma^2_{\log_{10} T_2}$: It is seen that the estimated uncertainty compares reasonably well with the true uncertainty obtained with the MT method. On the other hand, the estimated uncertainty of this parameter from the ILT method is very large. The ILT method not only overestimates the width but also has a huge variance in this parameter. For example, for model A at high SNRs, the width from the MT has an error-bar of 13%. The estimated error-bar based on SNR of the data is 12% and matches the true error-bar quite well. On the other hand, the error-bar from the ILT is 96%.

The simulation results described in this section are representative of results on a number of models at varying SNRs and for different values of α in Eq. (2). In summary, as seen in Eqs. (23), (24) and Fig. 9, the MT is sensitive to the input porosity. When the porosity is estimated well, the MT outperforms the ILT with a lower bias and variance of the estimated parameters. On the other hand, the results from the ILT method are systematically biased. The mean of the T_2 distribution is smaller than the true value. The width of the T_2 distribution is systematically larger. These results are illustrated in Fig. 15. The estimated T_2 distributions from data simulated from Model A with 10 different noise realizations with $\sigma_\epsilon = 0.02$ are shown. The bias seen in the previous results for the ILT case are, to a large extent, caused by artifacts at the beginning of the estimated distributions, which result in a decreased mean and increased width for the T_2 distribution.

5. Summary

This paper describes a new method to compute moments of the transverse relaxation time T_2 from measured CPMG data. The new method is based on the Mellin transform of the data and its

Table 3
Results of analysis of 1024 data sets at two different SNRs for different models using MT and ILT methods.

Model	Parameters	True value	High SNR			Low SNR		
			MT	ILT	Est.	MT	ILT	Est.
A	$T_{2,LM}$ (ms)	667	669	646		641	583	
	$\sigma_{T_{2,LM}}$ %		1	4	0.4	5	8	3.7
	$\sigma^2_{\log_{10}T_2}$	0.02	0.02	0.05		0.03	0.1	
	$\sigma_{\sigma^2_{\log_{10}T_2}}$ %		13	96	12	66	68	57
B	$T_{2,LM}$ (ms)	883	903	855		879	778	
	$\sigma_{T_{2,LM}}$ %		1	4	0.5	8	11	4.1
	$\sigma^2_{\log_{10}T_2}$	0.1	0.09	0.13		0.1	0.19	
	$\sigma_{\sigma^2_{\log_{10}T_2}}$ %		3	31	3	23	35	20
C	$T_{2,LM}$ (ms)	18	24	21		30	22	
	$\sigma_{T_{2,LM}}$ %		3	7	0.8	9	12	5.2
	$\sigma^2_{\log_{10}T_2}$	0.43	0.15	0.28		0.08	0.28	
	$\sigma_{\sigma^2_{\log_{10}T_2}}$ %		6	15	3	31	18	31
D	$T_{2,LM}$ (ms)	300	303	291		291	263	
	$\sigma_{T_{2,LM}}$ %		1	4	0.5	6	8	3.8
	$\sigma^2_{\log_{10}T_2}$	0.04	0.03	0.07		0.05	0.12	
	$\sigma_{\sigma^2_{\log_{10}T_2}}$ %		7	61	7	43	48	38

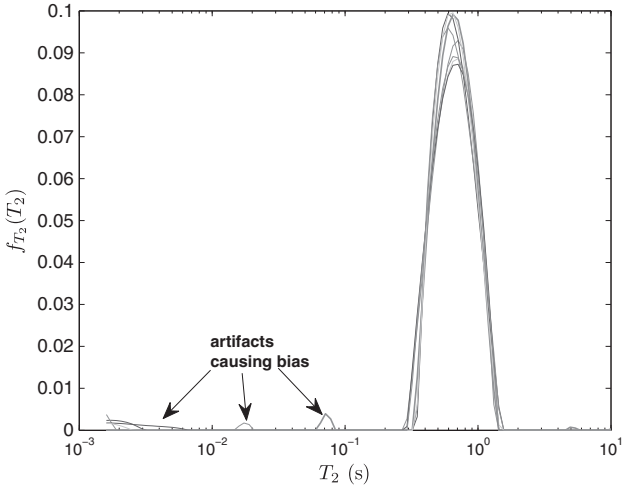

Fig. 15. Estimated T_2 distribution for 10 realizations of noise corresponding to Model *2*. The plot shows the artifacts at the beginning of the distribution that cause the bias in the results seen in previous plots.

time-derivatives. This method can also be used to generate the cumulant generating function of $\ln T_2$ directly. The inputs to the MT are the measured magnetization data and the porosity. The output of the MT are the moments of relaxation time, the cumulant generating function $G(\omega)$, as well as uncertainties in these parameters.

We discuss the properties and numerical implementation of the transform. The transform is linear and computed in a straight-forward manner. It takes, on an average, about a fraction of a second of CPU time to compute the parameters on a laptop D600PC with a 2.6 GHz processor.

The performance of the algorithm is compared with the traditional ILT method on simulated data. It was found that the MT method performs better than the ILT method when the porosity is well-determined. The ILT method often underestimates $T_{2,LM}$ and overestimates the width.

The relation between the SNR and the uncertainty in parameters such as $T_{2,LM}$ and the width of T_2 distribution has always been unclear. For example, if the SNR is an order of magnitude better, is the uncertainty in $T_{2,LM}$ about an order of magnitude lower? Analytic expressions for the uncertainty derived in this paper can help address this issue by relating the uncertainty in moments to the SNR in the data.

References

[1] R.L. Kleinberg, Encyclopedia of Nuclear Magnetic Resonance: Chapter Well Logging, vol. 8, John Wiley, 1996.
[2] G.C. Borgia, R.J.S. Brown, P. Fantazzini, Different average NMR relaxation times for correlation with fluid-flow permeability and irreducible water saturation in water-saturated sandstones, J. Appl. Phys. 82 (9).
[3] D.E. Freed, Dependence on chain length of NMR relaxation times in mixtures of alkanes, J. Chem. Phys. 126 (2007) 174502.
[4] J.G. McWhirter, E.R. Pike, On the numerical inversion of the Laplace transform and similar Fredholm integrals of the first kind, J. Phys. A: Math. Gen. 11 (1978) 1729–1745.
[5] C.L. Epstein, J. Schotland, The bad truth about Laplace's transform, SIAM Rev. 50 (2008) 504–520.
[6] E.J. Fordham, A. Sezginer, L.D. Hall, Imaging multiexponential relaxation in the $(y, log_e T_1)$ plane, with application to clay filtration in rock cores, J. Magn. Reson. A 113 (1995) 139–150.
[7] L. Venkataramanan, Y.-Q. Song, M.D. Hürlimann, Solving Fredholm integrals of the first kind with tensor product structure in 2 and 2.5 dimensions, IEEE Trans. Signal Process. 50 (2002) 1017–1026.
[8] P.C. Hansen, Regularization tools – a Matlab package for analysis and solution of discrete ill-posed problems, Numer. Algorithms 6 (1994) 1–35.
[9] J.P. Butler, J.A. Reeds, S.V. Dawson, Estimating solutions of the first kind integral equations with nonnegative constraints and optimal smoothing, SIAM J. Numer. Anal. 18 (3) (1981) 381–397.
[10] G. Wahba, Constrained Regularization for Ill-posed Linear Operator Equations, with Applications in Meteorology and Medicine, Technical Report, University of Wisconsin-Madison.
[11] J. Honerkamp, J. Weese, Tikhonov regularization method for ill-posed problems, Continuum Mech. Thermodyn. 2 (1990) 17–30.
[12] L. Venkataramanan, T.M. Habashy, D.E. Freed, Continuous moment estimation using fractional calculus, Submitted to Inverse Problems x (2009a) yy–yy.
[13] L. Venkataramanan, T.M. Habashy, D.E. Freed, Properties of Mellin transform in continuous moment estimation, Submitted to Inverse Problems x (2009b) yy–yy.
[14] I.S. Gradshteyn, I.M. Ryzhik, Table of Integrals, Series and Products, Academic Press, 2007.
[15] M. Prange, Y.-Q. Song, Quantifying uncertainty in NMR T_2 spectra using Monte Carlo inversion, J. Magn. Reson. 196 (2009) 54–60.